Improving Ozone Layer Depletion Forecasting with Hybrid Bi-Directional LSTM with CNN Classifier Model

JAVED ALI

College of Computing and Informatics, Saudi Electronic University,

11673 Riyadh, Saudi Arabia. j.ali@seu.edu.sa

ABSTRACT

Due to the methane emission from the mining of coal and industrial byproducts including CFCs, depletion of the ozone layer causes raised global warming and worsens climate change. One chlorine atom can lead to the destruction of 1,00,000 ozone molecules causing depletion at a much faster rate than natural replacement. The research studies the impact of industrial expansion of Delhi on ozone depletion through the development of hybrid predictive modeling by the integration of Convolutional Neural Networks (CNN) and Bi-directional Long Short-Term Memory (Bi-LSTM) networks. While the CNN extracts important spatial features, the Bi-LSTM captures temporal dependencies, thus achieving precise forecasts. To further improve the extraction of relevant data from encoded sequences, a multi-head attention layer is placed between encoder layers. The model performance was assessed using Mean Absolute Error (MAE), Root Mean Square Error (RMSE) and Normalized Root Mean Square Error (NRMSE). The simulation results indicate that the CNN-Bi-LSTM model is characterized by a MAE of 0.214, an RMSE of 0.268, and a MAPE of 34.22%, and esteems it to be better than the traditional models, such as LSTM, SVR, and Random Forest. The model predicts ozone depletion for short and long periods of time, thus ensuring accurate future projections and reliable monitoring. The developed system was tested in various conditions for 2100 hours and found to be accurate, reliable, and robust. These findings would indicate the suitability of the system for real-time monitoring and forecast at an appropriate time for policy intervention and recommendation to minimize further depletion.

Keywords: Air Pollution, Convolution neural network, Delhi Regions, Long short-term Memory, Ozone Layer Depletion, Ozone Layer Monitoring.

1. INTRODUCTION

In recent years, ozone depletion is the dangers to the earth faces, which has the effect of increasing the amount of different solar rays, including ultraviolet rays, which are entering the atmosphere. Specifically, it has a significant impact on the health of a variety of living species, with the skin being the most affected. The creation of the ozone hole and its ongoing expansion can be attributed to a number of different factors. Recently, a noticeable increase in awareness, and governments from a variety of countries have expressed their concern regarding this matter. Additionally, it is one of the factors that contribute to various forms of pollution, agricultural risk, climate change, and global warming, all of which have the potential to have an indirect influence on life on earth [1]. When it comes to pollution, for example, the use of high-resolution quality of air models in the Andes Region is quite limited. This is especially true in the medium-sized towns of South America, which are experiencing rapid urbanization, which in turn raises the risk associated with air pollution periods [2].

For the same reason, determining the extent of the ozone (O3) threat to vegetation is essential for informing policy decisions in the context of agricultural concerns. The availability of both phosphorus and nitrogen in the soil has the potential to alter stomatal conductance, which is the primary factor in the capacity of a leaf to take in oxygen. Additionally, the availability of both phosphorus and nitrogen could have an effect on photosynthesis and growth, which would result in a change in the sensitivity of plants to oxygen based on the quantities of nitrogen and phosphorus in the soil [3]. To be more specific, humans have been responsible for the emission of ozone-depleting chemicals (ODSs), which has resulted in the continual depletion of the ozone layer on a worldwide scale. This has resulted in significant concerns for both the environment and the human population. In light of this, it is essential to investigate the impact of each unique ODS in order to make an estimate of the ways in which this load may shift in the future [4].

Solar radiation and related meteorological variables are other environmental elements that have substantial impacts, alongside ODSs. Because of its impact on energy production, food safety, the ozone layer, and other industrial applications, solar radiation and related climatic variables have garnered increasing attention over the years. Therefore, numerous places have made it a priority to study how to forecast these factors both in the long and short term utilizing different fusions of recorded meteorological parameters. But it's still not easy to create and choose a reliable model to

estimate solar radiation using a number of weather characteristics [5]. The present review compiles what is known so far about the interplay between climate change and ozone-depletion as it pertains to aquatic ecosystems, specifically how these two factors influence UV radiation exposure in both freshwater and saltwater environments. Additionally, it discusses the ways in which the loss of ozone in the stratosphere is influencing southern hemisphere climate and the far-reaching consequences this has on aquatic environments [6].

Continuing to reduce the ozone-depletion gases concentration in the atmosphere is essential to the process of restoring the ozone layer in the stratosphere. The second-most prevalent trichlorofluoromethane (CFC-11), chlorofluorocarbon, has seen a significant decrease in atmospheric levels since the second half of the 1990s. On the other hand, there has been a halt in the reduction of CFC-11 air concentrations after 2012, which indicates that emissions on a worldwide scale have accelerated [7]. Since the 1970s, the amount of ozone in the Earth's isothermal layer has been steadily declining, falling by five percent every decade. There is a growing ozone hole in Antarctica and other rarefied ozone regions due to the widespread usage of chlorofluorocarbons in modern industries. Since the 1980s, a number of meteorological satellites have been launched by several national space ministries to track this topic of environmental change. Unfortunately, scientists typically manually record such ozone hole data from satellites, which is a rather wasteful process [8].

Increased manufacture and usage of elements that consist of chlorofluorocarbons (CFCs), halons, and other compounds comprising both bromine and chlorine, which are commonly referred to as ozone-depleting substances (ODSs), have been the primary contributors to the loss of the ozone layer in the stratosphere, which was first seen in the 1980s [9]. Within the context of the Montreal Protocol (MP) and the United Nations Sustainable Development Goals, the interacting impacts of solar ultraviolet (UV) light, climate change, and the stratospheric ozone layer are discussed. Topics covered include the effects of climate change on air and atmospheric quality, biogeochemical cycles, solar power, human wellness, materials used in outdoor building, and fabrics, as well as ecosystems of both land and water. Changing seasonal patterns and more frequent and severe weather events are two ways in which climate change is already having an impact [10].

Many people die each year as a result of air pollution, which is one of the biggest threats to human health in the modern era. The ozone layer is one of our most dangerous atmospheric pollutants

among many others. Breathing heavily, asthma, inflammatory disorders, and premature death are all examples of the serious health problems it can bring about [11]. As the amount of biologically effective solar UV, that reaches Earth's surface increases due to ozone depletion, remote sensing has been essential in understanding the impacts of this phenomenon on biogeochemical cycles around the world [12].

The worldwide map of ozone concentration is one of the two components that are included in Figure [1]. The color scale on this map ranges from 100 to 500 Dobson units. The amount of ozone that is present in the atmosphere of the Earth is quantified using Dobson units, abbreviated as DU. The amount of ozone that would be required to produce a layer that is 0.01 millimeters thick at standard temperature and pressure (STP) is referred to as one Dobson unit. This layer would normally extend from the surface to the top of the ozone layer, which is approximately 20-30 kilometers above the surface of the Earth. The other is a diagrammatic representation of the ozone profile in the atmosphere, which shows the tropospheric ozone layer at the lower altitude and the stratospheric ozone layer at the higher altitude.

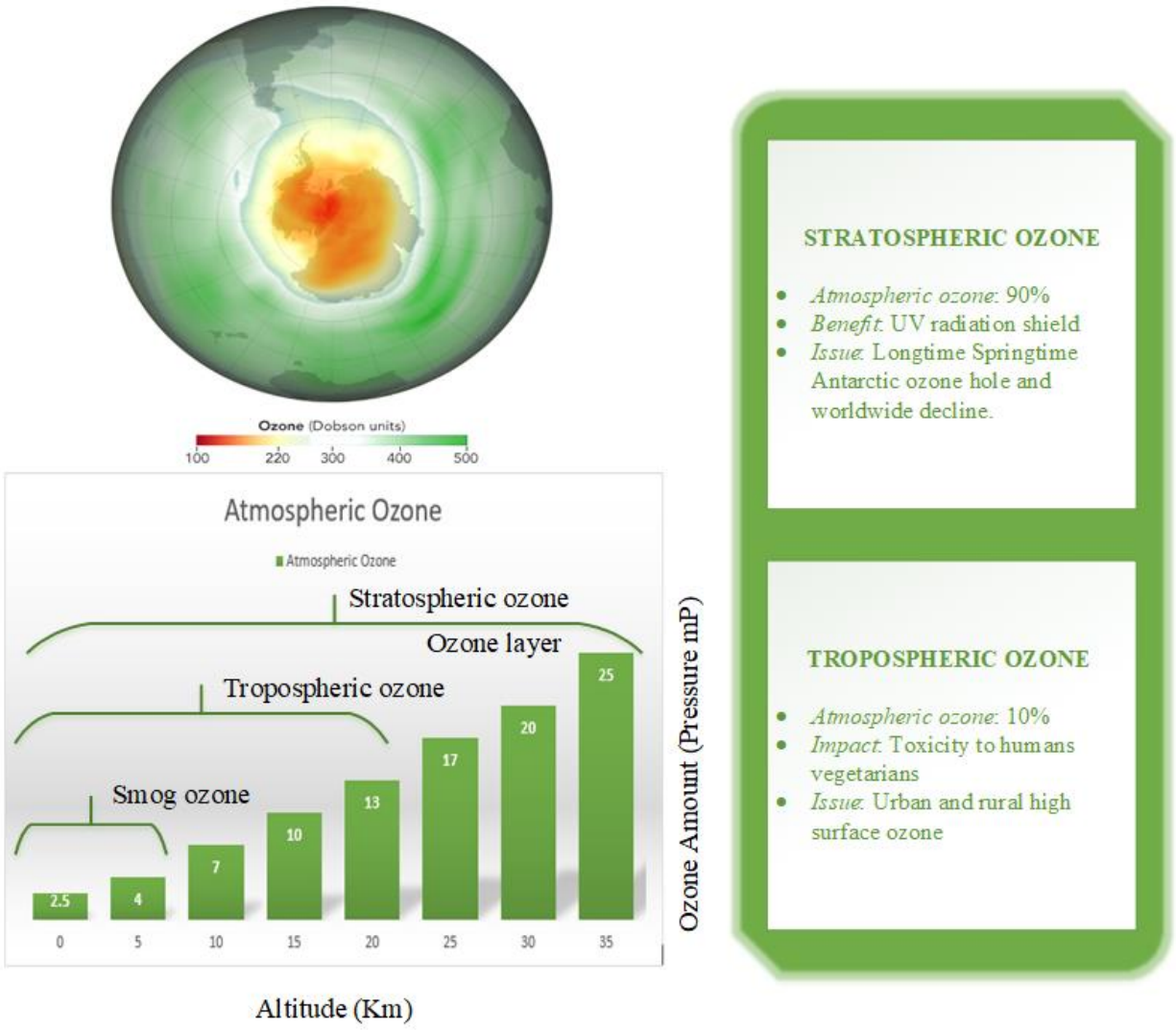

Figure [1]: Global Ozone Concentration Map and Atmospheric Ozone Profile Schematic

The Earth's stratospheric ozone layer is being depleted because ozone-depleting chemicals remain mostly unaltered in the lower atmosphere. Unfortunately, they are photosensitive and are dissolved to release free chlorine atoms because of this. Chlorine monoxide (CIO) and oxygen are byproducts of the reaction between this free chlorine atom and an ozone molecule (O3). After then, one ozone molecule reacts with ClO to produce an atom of chlorine and two molecules of oxygen. Perpetuating the cycle of ozone deterioration, the free chlorine atom can once again interact with ozone [13]. After the Montreal Protocol phased out the manufacture of ozone-depleting chemicals, the atmospheric concentration of CFC-11 began to decline. Suddenly, rising emissions since 2013 probably from undocumented production slowed the fall in CFC-11 quantity, which, if continued,

might postpone the recovery of the ozone stratospheric. Global mean CFC-11 concentrations, as measured in the atmosphere at several locations across the globe, are expected to fall sharply in 2019 and 2020, according to recent data [14].

Massive weather systems, like the Asian summer monsoon, sweep across most of Asia every summer. The Asian summer monsoon anticyclone (ASMA) carries pollutants from Asia's fast industrializing nations into the tropical upper troposphere, according to recent studies. A greater than anticipated mixing ratio of ODSs is being transported into the upper troposphere as well as lower stratosphere by the Asian monsoon, which is likely to have an effect on the stratospheric ozone layer [15]. Because of its high absorption capacity, O3 in the stratosphere protects life on Earth from the deadly ultraviolet (UV) rays that would otherwise reach the surface. Though nearly all ultraviolet light in the 200–280 nm band is absorbed, some of the 280–300 nm and 320–400 nm bands do reach the surface. Smoke from flames generated by nuclear weapons could induce climatic change that lasts up to fifteen years, endangering food supply, in addition to the immediate fatalities caused by the explosion, temperatures and radiation. This has the potential to deplete our ozone layer, which might take ten years to replenish, and then expose us to dangerously high levels of ultraviolet radiation at the surface for numerous years, posing a further threat to human wellness and availability of food [16].

As part of the UN Environment Programme, the Montreal Protocol's Environmental Effects Assessment Panel studies how variations in surface UV rays as well as changes to the stratospheric ozone layer affect ecosystems and human health. Scientific developments formed the basis for the most recent revision. The article goes on to talk about the interplay between climate change, UV radiation, and stratospheric ozone depletion, as well as the inverse relationship between the two. Air pollution, carbon sinks, ecosystems, human health, and synthetic and natural materials are used to evaluate the consequent interconnected impacts of ultraviolet radiation, climate change, and stratospheric ozone depletion. Gathering input characteristics that affect variations in ozone concentration is essential for creating an accurate prediction model. Consequently, it is necessary to construct a very accurate model with very few input parameters. The deterministic method and statistical regression are two of the many methodologies used to predict ozone depletion on a global scale. To identify ozone depletion, it is preferable to employ artificial intelligence methods, such as deep learning methods, which are far more effective while requiring less computational

time and resources. There have been advancements in the model of neural networks that offer a stable prediction method [17]. Hazardous air pollutants, namely benzene, toluene, ethylbenzene, and xylene (BTEX), are of grave concern for human health, which is a catalyst for the air-quality monitoring and control scheme [46]. Membranes from advanced polymeric nanocomposites, for instance, Pebax/PEG/NCS with high CO_2 selectivity and permeability, are also useful in the degradation of air pollutants [47]. These conclusions also underscore continuous ozone monitoring and prediction modeling as matters of importance in minimizing air pollution and impacts on climate. The proposed CNN-BiLSTM hybrid model enhances the prediction of ozone-depleting events in real time, leading to improvements in strategic environmental policymaking and public health safety.

The context of this study highlights the significance of the ozone layer in shielding life on Earth from damaging UV radiation and the role that industrial pollution plays in hastening its depletion. The previous monitoring techniques lacks in precisely forecasting and monitoring the ozone depletion over time. To address this research gap, the cutting-edge hybrid strategy is proposed for ensuring the real-time ozone monitoring. The motivation of this study is to address the ozone layer's continuous depletion, that mostly caused by human activities as coal mining and industrial pollutants. A hybrid predictive model is designed, which involves CNN and Bi-directional Long Short-Term Memory (Bi-LSTM)-based prediction for more effective ozone depletion forecasting than traditional models. While CNN networks extract shallow spatial features, Bi-LSTM networks capture long-term temporal dependencies, thereby enhancing predictive performance. A first-of-its-kind application of multi-head attention layer integration between encoder blocks enhances the model capacity to focus on important parts of the encoded sequences, thus improving its performance. The model also dynamically adapts to environmental data and assures continuous ozone monitoring with higher efficacy, reliability, and robustness.

2. RELATED WORKS

In the article [18], the authors utilized simulations demonstrate that the emission of sulphur into the stratosphere as a result of the Toba supereruption 74,000 years ago produced a significant loss of ozone in the stratosphere. This loss was induced by a radiation attenuation process that only modestly depends on the amount of the emission. In the tropical regions, where conditions of

extraordinarily low ozone levels persisted for more than a year, the Toba plume had a significant impact on the process of oxygen photolysis, which in turn served to suppress ozone synthesis. When this effect is combined with the phenomenon of volcanic winter in the extratropics, it is possible to explain the effects that supereruptions have on environments and people inside these natural environments.

Polar stratospheric clouds (PSCs) are newly discovered clouds that form in the polar stratosphere in the months of winter and first weeks of the spring when the air is still cold enough to allow clouds to be created despite the extreme dryness (as emphasized by the authors of [19]). As a result of these datasets, advancements have been made in understanding how PSCs are formed and their impact on atmospheric dynamics. Additionally, improvements have been made in how global models simulate intricate cloud processes. In the long run, this will result in improved forecasts for the rate at which the ozone layer in the stratosphere is recovering from the effects of human activity as the climate of the entire planet changes.

The study [20] examines regional CFC-11 concentrations from model simulations. In 2019, CFC-11 concentrations dropped 10 ± 3 gigagrams per year from 2014-2017, but they climbed back up to levels seen before 2013 in 2008-2012 (7.2 ± 1.5 gigagrams per year, ±1 standard deviation). In addition, it was found that pollutants of dichlorodifluoromethane (CFC-12) and carbon tetrachloride (CCl4), which could be linked to the manufacturing of CFC-11, were greater than anticipated after 2013 and then decreased in the year or two preceding the fall in CFC-11 concentrations. Taken together, the evidence points to CFC-11 manufacturing in eastern China following the worldwide phase-out that was authorized, with subsequent output falling in 2017 and 2018. Final estimates put eastern China's CFC-11 bank (the quantity of CFC-11 created but not yet emitted) at 112 gigagrams more likely due to increased production in the past few years.

Through the utilization of a multidimensional chemical transport model and satellite measurements, the authors of [21] conducted an investigation into the depletion of ozone in the Arctic over the winter months and spring months of 2019/20 and compared their findings to those gained from past years. The model simulation, which includes the peak recorded stratospheric total bromine and chlorine loading from the middle of 1990 demonstrates that the slow recovery of the ozone layer over the last two decades has helped to alleviate the polar cap ozone depletion that occurred in March 2020 by around twenty degrees below the equator. Furthermore, this model

was utilized to differentiate between the roles that transport and chemistry played in the process of creating the low ozone percentages. In addition, it provides a quantitative analysis of the magnitude of the ozone recovery signal in the Arctic region.

The researchers were primarily concerned with a peculiar increase in the levels of trichlorofluoromethane, also known as CFC-11, that were found in the air [22]. In addition, it was suggested that China has reduced the amount of an ozone-depleting chemical that it was producing, which is a positive development for the international accord to protect the ozone layer. An atmospheric travel model was developed as a method of facilitating the identification of the primary contributor to rogue emissions and the implementation of actions to control the generation of these emissions.

Within the framework of [23], the authors detailed the creation and implementation of feedforward neural network models that could be utilized for making predictions one day in advance regarding the maximum 1-hour ozone concentration (1hO3) and 8-hour average ozone concentration (8hO3) at one traffic and one background station in the Novi Sad, Serbia urban area. Ozone concentrations from the day before the forecast, the number of days in the year, the number of weekdays for which the ozone prediction was made, and the six meteorological variables from the day before the predicted event and the day of the prediction itself were all used as inputs.

The study [24] aims to create a supervised model for air pollution prediction using actual sensor data and transfer the model between cities. To predict the concentration of air pollutants in various parts of a city utilizing spatial-temporal correlations, a convolutional neural network and a long short-term memory deep neural network model were combined. Two strategies have been used: the multivariate model incorporates information on all contaminants and meteorological data for forecasting, whereas the univariate model only includes information on one pollutant. To evaluate the quality of ambient (outside) air, a thorough investigation is necessary, based on observations of the concentrations of the main pollutants obtained from several monitoring stations.

To achieve this goal, the investigators of [25] put forth a model based on ensembles to evaluate the air quality in from 2000 to 2016. Here, we used ensemble approaches to fix problems with imbalanced dataset preliminary processing and boost system efficiency overall. We checked the suggested model against the ones that were already out there. Experimental results show that the suggested model performs better than competing systems in terms of accuracy and error rate.

As proposed in [26], a clustering-based spatial transfer learning Multilayer Perceptron (SPTL-MLP) can be used to predict the ozone concentration at the target observation station over the next three days. The k-means clustering technique was then used to find comparable stations and train them together, resulting in a rudimentary model for spatial transfer learning. For real-world applications, a weighted loss function has been created with an emphasis on reducing mistakes in the prediction of high ozone concentrations. When employing historical data from German stations, the SPTL-MLP model offers greater prediction accuracies of ozone exceedances (improved by 8.21% and 16.9%) and a smaller error (reduced by 9.13%) than MLP (without spatial transfer).

The CNN-Transformer model is a hybrid model that was proposed by the authors of [27] and is based on a CNN technique and a Transformer model. This model was designed to predict the ozone concentration. As a result, it is clear that this model performs better than other models because it produces exceptional results on both the short-term forecast (RMSE = 7.75) and the long-term forecast (RMSE = 16.27).

On this hybrid model approach, the researchers of [28] also suggested using a Bayesian Optimized CNN-RNN hybrid model to accurately forecast when the air quality will be at its worst. This would allow them to take preventative measures to reduce the amount of pollution that is coming into the environment. To circumvent the issues that are typically associated with the manual modification of hyperparameters in neural networks, the researchers concluded that this technique would be the most effective. Both of these algorithms are examples of machine learning. When all was said and done, the BO-CNN-RNN was capable of outperforming the other models, and it did so even better as the predictions were made further beyond the present.

The research presented in [29] undertakes an analysis of consecutive measurements of O3 and NOx (NO+NO2) levels to enhance our comprehension of the development of ozone over the summertime of 2017 to 2019. To capture the variability of O3 and NOx concentrations, the k-means clustering technique was utilized to choose five typical data collection locations for air quality monitoring in Tehran. The results of the investigation indicate that none of the locations that were looked into were able to satisfy the ozone non-attainment requirement. In the examination of differences between weekdays and weekends in the years 2017, 2018, and 2019, the ozone weekend impact was observed. However, in 2019, this effect was not observed, which

may be related to a change in the production regime for ozone. The examination of the summertime mean variation can also be utilized to infer the existence of this regime change.

The researchers of [30] took ambient air samples at 20 different places in the PRD region during the winter (November to December 2019) and summer (August 2020) seasons. Their objective was to gather pertinent data and improve their understanding of the ODS emissions situation in the PRD region. In order to assess the emissions of ozone-depleting compounds (ODS) and ascertain their spatial-seasonal variability, this sample was examined. Following the analysis, the researchers showed that, with the exception of CFC-114, which largely remained at the same level throughout the entire observation, the average mixing ratios of the target ODS in the PRD region were 16.5%–92.5% lower than their reported values in 2001.

The authors of [31] also detailed the process and features of CNN-ILSTM, a model for AQI prediction that combines CNN with Improved Long Short-Term Memory. To avoid learning supersaturation, ILSTM improves upon LSTM by eliminating its output gate and adding a Conversion Information Module (CIM) to its input and forget gates. Training time is reduced, accuracy in predictions is improved, and efficient learning of historical data is achieved via ILSTM. Effective eigenvalue extraction from input data is achieved via CNN. This model was tested using air quality data collected in Shijiazhuang City, Hebei Province, China, from 00:00 on January 1, 2017 to 23:00 on June 30, 2021. It was compared to eight other prediction models, after 85.3 seconds of training, the experimental findings reveal an MAE of 8.4134 for CNN-ILSTM, an MSE of 202.1923, and an R2 of 0.9601. The results of this experiment show that this model outperforms the others.

However, an effective, reliable, and exceptionally precise additive hybrid model was used by the writers of the aforementioned work [32]. For the purpose of AQI forecasting, this model is introduced as an additive-ARFIMA-SVM, which combines a Support Vector Machine and an Autoregressive Fractionally Integrated Moving Average with functionally enlarged inputs. In addition, a meta-heuristic approach based on the group best leader strategy (GWOA-GBL) was suggested for optimization of gradient whales. In addition, the ARFIMA-SVM model outperforms SVM (43.47%), LSTM (40.39%), ARIMA (16.34%), Multiplicative-ARIMA-SVM (8.64%), ARFIMA (14.47%), and XGBoost (33.96%), when taking symmetric mean absolute percentage error into account.

The research team of [33] recommended MPR-RSA and EAQP, which stands for ensemble-based air quality prediction, as a way to build an automated system for predicting air quality. Methods including data cleansing, data transformation, and data imputation are used to accomplish the preliminary processing. The important features extracted from the preliminary information. Statistical, geographical, and temporal features are used for extraction. The suggested MPR-RSA algorithm optimizes the weight parameter, which is used in weighted feature selection to increase predictive accuracy. Afterward, EAQP completes the classification process by optimizing the hyper-parameters using the same MPR-RSA technique. Support vector regression, recurrent neural networks, extreme learning, bidirectional LSTM, and MLP neural networks are the individual Prediction approaches used to build the ensemble model in this case. In the end, we look at the performance with several parameters, and we find that the RMSE is 9.96%, which is lower than some of the various heuristic algorithms out there. Consequently, the suggested prediction model achieves low MAE and RMSE values, providing prompt predictions of ambient air pollution to avoid environmental harm.

Finally, researchers analyzed a dataset on CO2 emissions using deep learning, univariate and multivariate time-series models, and advanced machine learning approaches in the study [34]. Coal supply statistics, CO_2 emissions, peak demand, and peak met are all part of the dataset that was retrieved from the central power authority. Various performance metrics have been employed to assess the efficacy of the implemented models. These metrics include MAE, MSE, SMAPE, RMSPE, RAE, RMSE and MAPE. To do training and testing, the researchers made use of a dataset that covers the years 2005 to 2021. In addition, they have projected CO_2 emissions from 2022 to 2050 using the top-performing models.

Emission from river-atmosphere interaction has remained an interesting area of research over the years. However, efforts to effectively estimate CO_2 fluxes from rivers have been complicated by spatial and temporal variability [48]. It will also help in better climate predictions by understanding the altitude effect of stable isotopes and how it is controlled by the moisture sources that are complicated in the high mountains [49]. Drought characterization in global river basins states the trend toward increasing severity and duration of droughts mainly in high-latitude regions [50]. Advanced air pollution monitoring models using images, such as IAPM, involve multiscale perception for high detection accuracies, thus providing brilliant opportunities for innovations in

the real-time assessment of environments [51]. Bayer red mud and yellow phosphorus emulsions have excellent desulfurization and denitration potential, which can greatly reduce SO_2 and NOx emissions from industrial sources [52,53]. Additional studies concerning phosphorus migration in reservoir sediments, when micro-pressure conditions are imposed, increase phosphorus release, particularly from Fe-P-S cycling, which may potentially lead to harmful algal blooms [54]. It throws light on safe disposal and resource recovery with CO_2 atmospheres enhancing the alcohol production and reducing harmful emissions under the pyrolytic digestion of vancomycin fermentation residue (VFR) under varied atmospheric conditions [55]. These point to the need for the installation and integration of these advanced technologies for environmental monitoring and pollutant control in addressing some of the most urgent problems facing the ecology today.

3. METHODS AND MATERIALS

3.1. Methodology

One of the main causes of ozone layer's thinning is discharge of harmful gases into the atmosphere. The ozone depletion significant factors are industrial emissions, creation of chlorofluorocarbons (CFCs) from refrigeration and aerosol propellants. Methane gas released by coal mining operations that harms the stratosphere layer makes the issue worse. The production of bromine and chlorine atoms from the industrial processes speeds up decomposition of ozone molecules, that becomes crucial for preventing damaging UV rays. These substances accelerate the rate of ozone depletion by significantly disrupt the natural equilibrium of ozone replenishment. The nitrous oxide and halons gases also can destroy the ozone layer due to the Industrial operations, aerosol propellants, and agricultural method that produce these gases. International agreements as Montreal Protocol controls the manufacture and utilisation of compounds might deplete the ozone layer. Another initiative is an adoption of ozone-friendly substitutes for industrial and agricultural practices.

Part one of the ozone layer depletion system is data pre-processing, part two is training the model, and the final part is evaluating it on test sets. As a first step, the raw data pre-processed to transformed into training-style data, which includes labeled data and input sequence data. After that, dimensional impacts between features are removed using a min-max normalizing method. Train the Bi-directional LSTM algorithm's encoder and decoder layers using the normalized input data. Ozone depletion solely serves as a univariate variable in the course of training, although multivariate data is also used. In the end, the CNN-Transformer model's efficiency is evaluated by

applying the trained model to the test set, renormalizing the outputs, and comparing them to labeled measurements. A structural representation of the deep learning model that has been proposed for ozone layer prediction is depicted in Figure [2]. An input layer, an imputer layer, a convolutional neural network, a dropout layer, a Bi-LSTM network, an output layer, and a prediction layer are the components that make up this system.

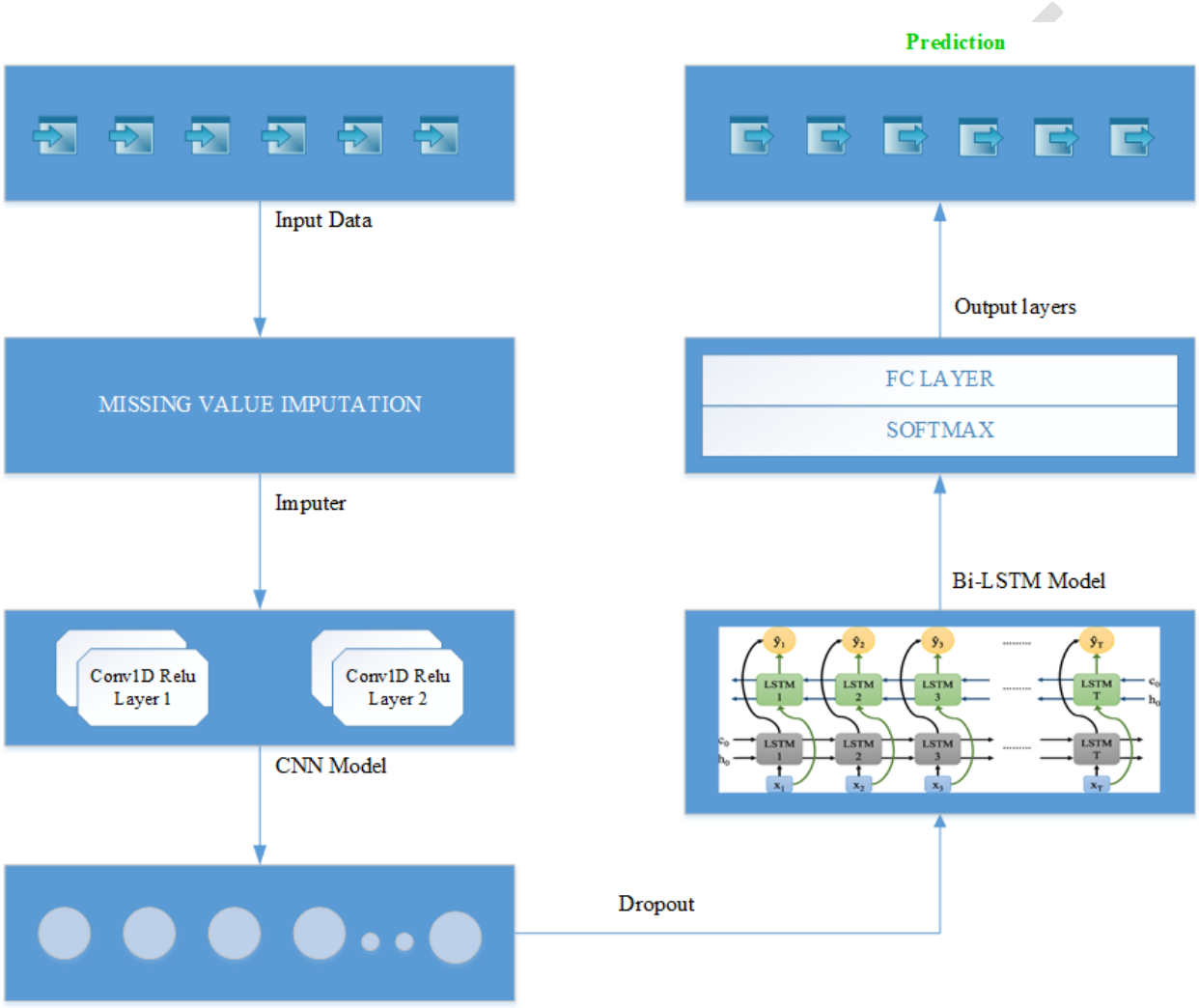

Figure [2]: Proposed Architecture of the Deep Learning Model for Ozone Layer Prediction

- **Univariate dataset:** When we are constructing the dataset, we simply give the ozone concentration feature to the time intervals. We divide the data into two halves, each with its own unique sequence, by introducing a sliding window of length N+1. The examples will compare the outputs of the CNN-Transformer model based on T_1,⋯,T_(m+N-1), with T_(m+N) serving as labeled data and T_m, ⋯, and T_(m+N-1) as historical data.

Once we've inspected all the data, we'll generate the next sequential sample by sliding the window one step at a time. With n being the length of the sequence and S_i being the i th sample, the sliding window has a length of 3.

- **Multivariate dataset:** When we are constructing the dataset, we make the assumption that the number of features, also known as dimensionality, is L at time T_m. We next express the data as a vector with the values T_m1, T_mL. The approach for the univariate dataset and its sliding window method also applies to the subsequent steps, which are very similar to one another. We present 9 features that are included in the multivariate dataset. These features are as follows: highest and lowest temperatures, CO, NO, SO_2, NO_2, wind (speed and direction), and ozone concentration. utilizing a window size of three, a sequence length of n, and a feature size of m at the same time. For the i th sample, the notation S_i is used.

3.2. Data Preprocessing

We convert raw past information into a format needed for the next training stage during data preliminary processing. The raw data is transformed into various sequences along two dimensions such as the time dimension and the feature dimension. The sliding window technique is used to construct both univariate and multivariate datasets in our work. The feature dimension is significant for collecting different data attributes which affects ozone layer depletion. The feature space extended by the model that precisely captures the intricacy of environmental elements that affects ozone layer variations, as temperature, humidity, UV rays, and industrial pollutants. More accurate predictions offered by the model's ability to identifies an complex correlations in the data by the larger feature dimension.

3.3. Methods Using Artificial Intelligence to Identify Ozone Depletion

3.3.1. SVR

The theory of statistical learning serves as the foundation for the machine learning technology known as support vector machine. There are several applications for time-series prediction that make use of SVR, which is a type of SVM. Some examples of these applications include load prediction, weather prediction, and fault prediction. Additionally, the SVR is utilized for the purpose of monitoring the temperature of the ocean. Because of this, the SVR can be

utilized for the depletion of the ozone layer. To monitor the depletion of the ozone layer, this work utilizes the SVR model. Assume a time-series data set that is presented as follows:

$$D = \{(X_i, y_i)\}, \text{ where } 1 \leq i \leq N \quad (1)$$

In equation (1), X_i refers input vector, that comprised of m elements, and y_i represents the value that is obtained as a result. In light of this, the regression formula can be stated as:

$$f(X_i) = W^T \phi(X_i) + b \quad (2)$$

In equation (2), W represents the weight vector, $\phi(X_i)$ utilized to map input data to higher-dimensional features, b refers bias. It is possible to acquire the answer to the optimization problem that is posed by W and b by using the following formula:

$$\frac{1}{2}|W|^2 + C\sum_{i=1}^{N} (\varepsilon_i + \varepsilon_i^*) \quad (3)$$

Subject to:

$$\begin{gathered} y_i - W^I(\phi(x)) - b \leq \zeta + \epsilon_i \\ W^I(\phi(x)) + b - y_i \leq \zeta + \varepsilon_i' \\ \epsilon_i + \varepsilon_i' \geq 0 \end{gathered} \quad (4)$$

In equation (3) and (4), the symbol 〈 is used to indicate the threshold, while C denotes parameter that represents the relationship between the simplicity of the model and its capacity to generalize. Additionally, ϵ_i and $\varepsilon_i'$are the slack variables that are used for determining the cost of errors.

3.3.2. ANN

Artificial neural networks (ANNs) are extensively employed in many different applications, such as rainfall and electricity demand forecasting. An ANN is a learning model that draws inspiration from the structure and operation of the brain's internal nervous system. Learning patterns is the responsibility of a hidden layer in ANN. Nonetheless, a single-hidden layer feedforward neural network (SLFN), the most basic ANN model, can be constructed using only one hidden layer. This single-layer network consists of an input layer, a hidden layer, and an activation function. Calculating the output of this network is done as follows:

$$y = g\left(\sum_{j=1}^{h} w_{jo} v_j + \mathbf{b}_j\right) \quad (5)$$

In equation (5), the hidden layer output, v_j, is represented by the function f($\sum_{i=1}^{n} w_{ij} x_i + \mathbf{b}_i$), where X_i refers input, f, and g denotes non-linear activation function, n refer features count, h refers hidden layer counts, and w_ij refers weight

3.3.3. RF

When it comes to classification and regression, Random Forest (RF) is a combined learning strategy. Multiple prediction systems also use the random forest-based regression method. For this kind of issue, random forests typically employ bagging and random subspace approaches. Random forest methods frequently employ bagging. These ensemble approaches state that after training individual learning models with bootstrap samples taken from the initial training data, the results are combined. The random forest makes use of the built decision tree to pick m features out of a total of n characteristics. Once the features are partitioned across the feature axis, the feature impurity criterion is utilized.

3.3.4. DBN

Common deep learning models used nowadays include DBNs, CNNs, and stacked autoencoders. Among the many varieties of neural networks, the DBN is notable for its many hidden layers. To get the discriminant features, the DBN model uses an unsupervised feature extraction method. The next step is to build a supervised learning model on top of DBN. In a similar vein, stacked autoencoders are a specific kind of neural network that has multiple sparse autoencoder layers connected at the output layer. Each step's encoding is described as:

$$a^{(l)} = f\left(z^{(l)}\right) \quad (6)$$

$$z^{(l+1)} = W^{(l,1)} a^{(l)} + b^{(l,1)} \quad (7)$$

In equation (6) and (7), The activation function in layer l is denoted by a(l), the weighted sum of inputs for layer l is denoted by z^((f)), the weight value is denoted by W^((l,k)), and b^((L,k)].

3.4. Proposed Deep Learning Model for Prediction

In order to forecast when the Delhi Region's ozone layer will be depleted, we offer a deep learning algorithm. The proposed models selected due to their ability of precisely capturing the temporal and spatial data for ozone depletion prediction. CNN method is excellent in extracting insightful features from input data, while LSTM maintains the sequential dependencies for enhanced prediction accuracy. This hybrid approach ensures robust performance, outperforms other methods. In most cases, the issues with regression model forecasting can be stated as:

$$y = \mathcal{F}(x; \theta) \tag{8}$$

The forecasting scope involves the evaluation of influence of industrial operations, the possible results of the mitigation method, and projecting future ozone depletion levels depends on the historical environmental data. The model assists the forecasting of future patterns and offers a prompt actions by offering an insight with different variables interact over time. In equation (8), Using pairs of training samples, the pattern is learned using the parameters of the mapping function F{(x_n,y_r)|r=1,…R}, where x denotes input vector and y refers anticipated output. Minimize prediction mean squared error (MMSE). The MMSE function is stated as:

$$\varepsilon = \frac{1}{R}\sum_{r=1}^{R} \|\hat{y}_r - y_r\|_2^2 \tag{9}$$

In equation (9), the input class is represented by y and the projected output class is y ˇ. To learn the parameters, this work employs a method based on deep neural networks. In order to train their networks, deep neural networks use a feedforward neural network model that incorporates hidden units.

Pattern recognition relies heavily on recurrent neural networks (RNNs) with deep bi-LSTM networks. The RNN models store data for processing time-series data in a memory unit that is informed by contextual knowledge. On the other hand, RNNs have trouble with gradient-induced long-range dependencies. To get around this, scientists have developed a pattern that uses memory cells to tackle the dependency problem; this model is called LSTM. Three multiplicative gates aid in forgetting and data storage in the cell states in this paradigm. The whole suggested deep Bi-LSTM model for ozone layer depletion prediction is shown in Figure [2], which is provided above. This study employs a CNN-Bi-LSTM hybrid. The CNN layers receive input data that has been processed by the missing value imputation model. Following processing by Bi-LSTM layers, the

anticipated output is produced by fully connected layers based on the CNN layer's output. Two max-pooling layers follow two one-dimensional layers in the first module. The computational complexity of feature extraction is reduced by this combination. Because of the interconnected nature of the perceptrons, traditional approaches that employ MLPs (multilayer perceptrons) as feature extractors through feed forward neural network processes often fall short of the desired results.

CNNs are a subset of multi-layer perceptrons (MLPs) that do not necessitate inter-neuron communication. Each of these neurons is sized and stride-dependently linked to a certain area of the input data. In this case, we use CNN filters to detect the various sites by sharing parameters and weights. CNN layers use training-derived weights and biases to merge neurons. We feed the neurons several layer depletion settings in this model. After that, a non-linearity function is applied, and then the dot product operator. The model's architecture includes a fully linked layer, a pooling layer, and a 1D convolution layer [34-36]. CNNs take time series data in the form of one-dimensional data ordered as consecutive time instants as input. The input vector is supplied as $x = \{x_1, x_2, x_3, \dots x_n\}$ where $x_n \in R^d$ are the variables of dataset. The input layer depletion data with filter w∈R^d is used by the ID convolutional layer to build a feature map, where f represents the intrinsic features, using conv operators. It is possible to derive a new feature map f_m from an existing one by rewriting the expression as:

$$hf_i^{f'} = \tanh\left(w^f x_{zi+f-1} + b\right) \tag{10}$$

In equation (10), the bias is represented by b and $h \in R_{n-f+1}$, For each *f* in the input data, the filter hl is applied as $\{x_{1:f}, x_{2:f+1}, \dots, x_{n-f+1}\}$, resulting in a feature map as $hl = [hl_1, hl_2, \dots. hl_{n-f+1}]$. By combining the weighted inputs that have been compromised through multilinear transformation, the output of the convolution layer may be derived. In most cases, non-linear functions are preferable for learning than linear ones since linear transformations miss the intricate structure of input data. Each input is processed using the ReLU activation function in this study [37-39]. After that, the max-pooling layer processes the convolution layer's output, and then we apply it to each feature map individually to conduct down sampling, as $\overrightarrow{hl} = \max\{hl\}$. The most crucial features can be selected with the help of this process. We can define the result of the max-pooling layer as:

$$x_i' = \text{CNN}\ (x_i) \tag{11}$$

In equation (11), the input vector $x_i$comprises the layer depletion parameters, and the output of the CNN model, x_i', is then supplied to the Bi-LSTM network. Here is the representation of this structure:

$$i_t = \sigma\big(W_i([x_t, y_{t-1}])\big) \tag{12}$$

$$f_t = \sigma\left(W_f([x_t, y_{t-1}])\right) \tag{13}$$

$$o_t = \sigma\big(W_0(x_t, y_{t-1})\big) \tag{14}$$

$$g_t = \tanh\left(W_g([x_t, y_{t-1}])\right) \tag{15}$$

$$c_t = f_t \odot c_{t-1} + i \odot g_t \tag{16}$$

$$y_t = o_t \odot \tanh\,(c_t) \tag{17}$$

From equation (12) to (17), we express a variety of gate types, such as input, forget, output, and input modulation gates, using the variables i, f, o, g, and c [40–41]. The fully connected neural networks W_i, W_f, W_o, and W_g respectively, represent the input, forget, output, and input modulation gates, while σ represents the sigmoid function. The element-wise product is denoted by $\odot$. Traditional LSTM often only handles one-way sequences, which reduces their efficiency; however, data that can be processed in both directions can often yield useful insights. Therefore, we use Bi-LSTM, which combines both directions in the data sequence, to overcome these problems [42]. These bidirectional data processing aids in capturing each informational change on layer depletion data. The LSTM classifies the elements of the layer depletion parameter sequence x as $\{x_1, x_2, x_3, \ldots x_n\}$ in the forward direction and as $\{x_n, x_{n\ -1}, x_{n-2}, \ldots x_1\}$. in the backward direction [43]. During training, each of these components is taught independently, and then their results are combined by combining the two sets of training results. One way to put it is:

$$y(t) = y_F(t) \oplus y_B(n - t + 1) \tag{18}$$

In equation (18), the forward and backward directions are represented by y_F and y_B respectively; the integration operator is $\oplus$; and the expected output at time t is $y(t)$.

The proposed hybrid CNN and LSTM model has ability to handle the uncertainty influencing ozone layer depletion. These models dynamically adjusting the unpredictable character, trends and pattern in the data. Furthermore, CNN and LSTM's structure enables enhanced management of temporal and spatial uncertainty. While the variables change, the system has ability to handle the real-time environmental data ensures accurate forecasts. This adaptability nature ensures accurate forecasts despite the variability in contributing factors.

4. RESULTS AND DISCUSSION

The simulation parameters for the suggested model are displayed in Table 1 and include daily data of Delhi's ozone layer depletion from 2014 to 2021. Wind speed and direction, as well as lowest and maximum temperatures, are some of the meteorological variables that are considered. Other air pollutants, such as CO, NOx, and SO2, were also taken into account due to their possible impact on ozone layer depletions. Our main objective is to test how well Bi-directional LSTM and CNN can forecast the highest 8-hour average ozone layer depletions for a given day. When it comes to time series prediction challenges, we evaluate our model alongside LSTM, CNN, and Transformer-based models. Here is the outline of our experimental procedure: We start by finding out how long the time series data goes back. After that, we compare the suggested CNN-Transformer model to the previous models and assess its performance. The models are then evaluated using corresponding data sets for both short-term and long-term prediction. Here, we include the predictions for the near and distant future:

Short-term Prediction: Predicting the maximum 8-hour average ozone layer depletion for the next day based on past data within a specific time range is an example of short-term forecasting. To illustrate the point, if we have data from Monday through Saturday of a particular week, we may use it to forecast Sunday's ozone layer depletion.

- Long-term Prediction: Using previous data within a particular time frame, we can anticipate the maximum 8-hour average ozone layer depletion for the next three days. For example, ozone layer depletion from Friday to Sunday can be forecasted using a collection of historical data from Monday to Thursday. When testing predictions for the future, we

utilize a multivariate dataset; however, when testing predictions for the near future, we use either a univariate or multivariate dataset. Given the multi-factor nature of ozone layer depletion, the discrepancy in datasets can be understood. A perfect reflection of the interaction of the various elements cannot be achieved by relying solely on historical ozone layer degradation. Furthermore, concluding future ozone layer depletion only from past ozone layer depletion is typically not realistic.

Table 1: Simulation Parameters for Proposed Deep Learning Model

Simulation Parameter	Value
Number of epochs	2500
Number of hidden units	250
Batch size	120
Activation Layer	Relu
LSTM activation	Tanh
Training ratio	70%
Training function	Bayesian regularization
Learning rate	0.001
Loss function	Mean absolute error
Padding	Same
Activation function	Tanh

Table 2 lists simulation settings for ozone layer forecast methods. Four hidden layer nodes, a sigmoid activation function, and 100 epochs of training with a batch size of one produce verbose output at level two in the LSTM model. Three dense layers with 32, 64, and 64 nodes use the "msprop" optimizer in the Artificial Neural Network (ANN). SVR uses a RBF kernel with C=1.0 and gamma as "scale." To prevent overfitting, the Deep Learning-Based Water Quality Assessment (DLBL-WQA) method uses 32 filters, a kernel size of two, a ReLU activation function, an input shape of (13,1), and a dropout rate of 0.25 This CNN-LSTM model has 32 filters, a two-kernel size, a ReLU activation function, and a (13,1) input shape. The Random Forest model has 100

estimators, automatic feature selection, and bootstrap sampling. For comparison, the Linear Regression model is set to default values.

Table 2: Parameters of several methods for simulation

LSTM	Hidden layer $LSTM$ nodes $= 4$
	Batch size is 1, verbose is 2, and the activation function is sigmoid with 100 epochs.
ANN	optimizer = "msprop", Dense layers nodes $= 32{,}64$, and 64
SVM	$C = 1.0$, Kemel = rbf, gamma = "scale"
DLBL-WQA	input_shape $= (13{,}1)$, Filters $= 32$, kernel $= 2$, dropout $= 0.25$, activation function = "relu,"
Linear regression	Default
CNN-LSTM	input_shape $= (13{,}1)$, Filters $= 32$, activation function = " relu", kernel $=$ 2,
Random forest	bootstrap = true, n_estimators $= 100$, max_features = "auto"

We simply utilize the multivariate dataset for the long-term forecast in order to provide more accurate and useful predictions. For research involving short-term prediction, however, matching the model to historical data does help. To compare the performance of various models and assess the accuracy of the results, the following metrics are used: Scilicet, mean absolute error (MAE), root mean square error (RMSE), and normalized root mean square error (NRMSE).

Table 3: Performance Measurement

Parameter	Computation
Mean absolute error (MAE)	$\text{MAE} = \frac{1}{N}\sum_{i=1}^{N} \lvert y(i) - \hat{y}(i) \rvert$
Mean absolute percentage error (MAPE)	$\text{MAPE} = \frac{1}{N}\sum_{i=1}^{N} \frac{y(i)-\hat{y}(i)}{y(i)} \times 100\%$
Mean squared error (MSE)	$\text{MSE} = \frac{1}{N}\sum_{i=1}^{N} (y_i \hat{y}_i)^2$

Root mean square error (RMSE)	$\text{RMSE} = \sqrt{\frac{1}{N}\sum_{i=1}^{N} (y(i) - \hat{y}(i))^2}$

Table 3 presents the prediction performance results for various models, showing their respective various values. In the time-series sequence under consideration, the anticipated value and actual value at time t are represented by $y(i)$ and $\hat{y}(i)$.

Table 4: Methods for Improved Prediction Performance

Methods	MSE	MAE	RMSE	MAPE
CNN-BiLSTM (Proposed)	0.012	0.102	0.109	18.45
DLBL-WQA	0.015	0.115	0.117	20.32
LSTM	0.328	0.358	0.401	46.82
Support vector regression	0.491	0.596	0.711	54.28
Random forest	0.487	0.614	0.568	53.24
Linear regression	0.401	0.556	0.480	51.29
Artificial neural network	0.566	0.521	0.652	54.21

Table 4 shows summary of the performance metrics of various predictive modeling strategies that are utilized to forecast the depletion of the ozone layer. The goal of this experiment utilizes previous 10 days data to forecast the maximum 8-hour average ozone layer depletion for the next three days. Since historical data can only be used to determine seasonal or temporal trends, it is unreliable to feed the forecasting engine with data on ozone layer depletion alone. The forecasting algorithm will be too insensitive to detect a fast shift in other climatic conditions that impact ozone levels on a given day, leading to a cumulative error. So, to investigate how well long-term forecasts work, we exclusively employ multivariate datasets. Differentiation of prediction models is represented in Table 4; CNN-Bi LSTM (Proposed) is the best performer under most metrics. CNN-Bi LSTM has the lowest MSE of 0.012, MAE of 0.102, RMSE of 0.109, and MAPE of 18.45%, thus being considered, certainly, the best predictive model. DLBL-WQA follows this with MSE, MAE, RMSE, and MAPE of 0.015, 0.115, 0.117, and 20.32%, respectively. The LSTM model does try to show some predictive abilities, although with comparatively much higher error rates of MSE 0.328 and MAPE 46.82%. Both support vector regression and random forest models fall under almost similar results, with MAPE values of 54.28% and 53.24%, respectively, showing the poorest prediction ability. Linear regression and artificial neural networks were among the worst-

performing models with MAPE values above 51% and 54%, indicating their lower reliability within the confines of this study. The CNN-BiLSTM has, thus, shown the ability to minimize prediction errors while also outperforming other models. The feature extraction capabilities of attention-based models are drastically reduced as the time series data to be forecasted becomes longer, as this proves. Even though the CNN model gathered legitimate information, the encoder in the model still has a hard time recognizing and using it.

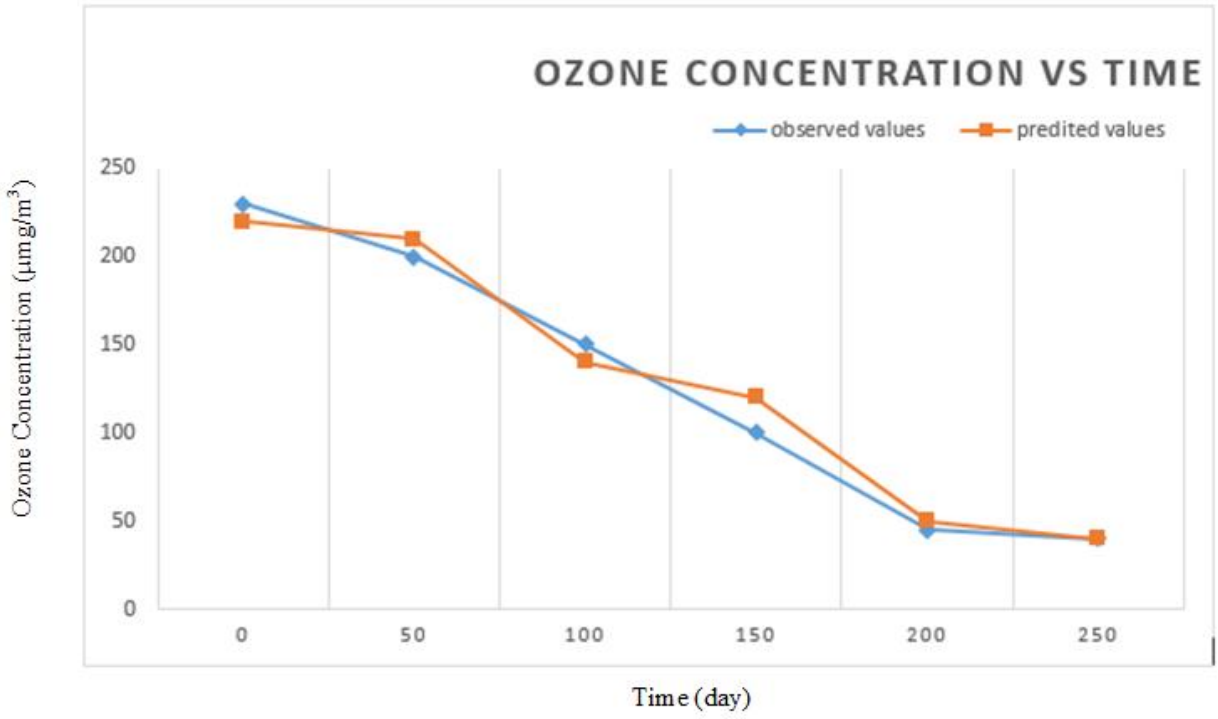

Figure [3]: Comparison of Predicted and Observed Ozone Concentrations

A comparison of the observed values and the CNN Transformer model's predicted values is displayed in Figure 3. Our model is more likely to disregard the potential causes of certain mutations since its attention mechanism learns global information, in contrast to the LSTM model. Even if the raw data is unstable, our model still performs admirably. In other words, with more trustworthy data, our model can guarantee accurate long-term prediction outcomes, but at the cost of model complexity. Future research could investigate and develop a new deep learning model to increase the algorithm's sensitivity to mutation spots and prediction accuracy.

5. CONCLUSION

This system is a prediction hybrid as far as ozone layer depletion prediction is concerned and has been proposed by us using the combination of the CNN model and the Transformer model for better accuracy of prediction. The CNN component takes advantage of the shallow as well as valuable features which hinders the encoder from learning other irrelevant information. The Transformer, further implementing a multi-head attention layer between several encoder layers, enhances the feature extraction more from the encoded sequences, capturing the short and long dependency states well along the short and long time. Outstanding performance was indicated with the proposed hybrid CNN-Transformer model across multiple datasets, registering MSE of 0.012, MAE of 0.102, RMSE of 0.109, and MAPE of 18.45% in comparison with the best-performing state-of-the-art models such as LSTM, CNN-Transformer, or DLBL-WQA. In contrast, the DLBL-WQA model achieved an MSE value of 0.015 with an MAPE of 20.32%. LSTM produced a lower predictive power reflected by MSE at 0.328 and MAPE of 46.82%. Nevertheless, it is unable to determine mutation spots or sudden changes in infiltration patterns of ozone depletion, and this limits the application of the model as the changes in environment suddenly might result in lesser accuracy. Also, the computational complexity that is involved in the multi-head attention in the transformer increases the training time and hardware requirements, which reduces its efficiency in real-time applications. Future work will target over these limitations by adopting an adaptive attention mechanism that would Peter be able to capture dynamic variations better and further reduce model complexity via optimized architecture. Further, real-time data assimilation addition to the system will be done along with further enhancing the anomaly detection techniques to further advance the reliability and applicability of the system in ozone layer depletion monitoring.

REFERENCES

1. Chakraborty, S., Sadhukhan, S., & Kumar, P. (2017). Dermatological effect of UV rays owing to ozone layer depletion. In 2017 4th International Conference on Opto-Electronics and Applied Optics (Optronix) (pp. 1-6). Kolkata, India. https://doi.org/10.1109/OPTRONIX.2017.8349975
2. González, C. M., Ynoue, R. Y., Vara-Vela, A., Rojas, N. Y., & Aristizábal, B. H. (2018). High-resolution air quality modeling in a medium-sized city in the tropical Andes:

Assessment of local and global emissions in understanding ozone and PM10 dynamics. Atmospheric Pollution Research, 9(5), 934-948. https://doi.org/10.1016/j.apr.2018.03.003

3. Zhang, L., Hoshika, Y., Carrari, E., Badea, O., & Paoletti, E. (2018). Ozone risk assessment is affected by nutrient availability: Evidence from a simulation experiment under free air controlled exposure (FACE). Environmental Pollution, 238, 812-822. https://doi.org/10.1016/j.envpol.2018.03.102
4. Singh, A. K., & Bhargawa, A. (2019). Atmospheric burden of ozone depleting substances (ODSs) and forecasting ozone layer recovery. Atmospheric Pollution Research, 10(3), 802-807. https://doi.org/10.1016/j.apr.2018.12.008
5. Abayomi-Alli, A., Odusami, M. O., Abayomi-Alli, O. O., Misra, S., & Ibeh, G. F. (2019). Long short-term memory model for time series prediction and forecast of solar radiation and other weather parameters. In 2019 19th International Conference on Computational Science and Its Applications (ICCSA) (pp. 82-92).
6. Williamson, C. E., Neale, P. J., Hylander, S., et al. (2019). The interactive effects of stratospheric ozone depletion, UV radiation, and climate change on aquatic ecosystems. Photochemical & Photobiological Sciences, 18, 717-746. https://doi.org/10.1039/c8pp90062k
7. Rigby, M., Park, S., Saito, T., et al. (2019). Increase in CFC-11 emissions from eastern China based on atmospheric observations. Nature, 569, 546-550. https://doi.org/10.1038/s41586-019-1193-4
8. Zhu, H., Theodoridis, S., Lam, K., & Lung, H. (2020). A new method for ozone depletion detection over Antarctica by deep convolutional neural network. In 2020 IEEE 5th International Conference on Signal and Image Processing (ICSIP) (pp. 506-511). Nanjing, China. https://doi.org/10.1109/ICSIP49896.2020.9339330
9. Chipperfield, M. P., Hossaini, R., Montzka, S. A., et al. (2020). Renewed and emerging concerns over the production and emission of ozone-depleting substances. Nature Reviews Earth & Environment, 1, 251-263. https://doi.org/10.1038/s43017-020-0048-8
10. Bernhard, G. H., Neale, R. E., Barnes, P. W., et al. (2020). Environmental effects of stratospheric ozone depletion, UV radiation and interactions with climate change: UNEP Environmental Effects Assessment Panel, update 2019. Photochemical & Photobiological Sciences, 19, 542-584. https://doi.org/10.1039/d0pp90011g

11. Aljanabi, M., Shkoukani, M., & Hijjawi, M. (2020). Ground-level ozone prediction using machine learning techniques: A case study in Amman, Jordan. International Journal of Automation and Computing, 17, 667-677. https://doi.org/10.1007/s11633-020-1233-4
12. Varotsos, C., Mazei, Y., & Xue, Y. (2021). On the contribution of remote sensing to the investigation of the effects of UV-B on mechanisms of ecology, biodiversity, and conservation. In 2021 IEEE International Geoscience and Remote Sensing Symposium (IGARSS) (pp. 6240-6243). Brussels, Belgium. https://doi.org/10.1109/IGARSS47720.2021.9554762
13. Aslam, B., Alrowaili, Z. A., Khaliq, B., Manzoor, J., Raqeeb, S., et al. (2021). Ozone depletion identification in the stratosphere through faster region-based convolutional neural network. Computers, Materials & Continua, 68(2), 2159-2178. https://doi.org/10.32604/cmc.2021.015922
14. Montzka, S. A., Dutton, G. S., Portmann, R. W., et al. (2021). A decline in global CFC-11 emissions during 2018–2019. Nature, 590, 428-432. https://doi.org/10.1038/s41586-021-03260-5
15. Adcock, K. E., Fraser, P. J., Hall, B. D., Langenfelds, R. L., Lee, G., Montzka, S. A., et al. (2021). Aircraft-based observations of ozone-depleting substances in the upper troposphere and lower stratosphere in and above the Asian summer monsoon. Journal of Geophysical Research: Atmospheres, 126, e2020JD033137. https://doi.org/10.1029/2020JD033137
16. Bardeen, C. G., Kinnison, D. E., Toon, O. B., Mills, M. J., Vitt, F., Xia, L., et al. (2021). Extreme ozone loss following nuclear war results in enhanced surface ultraviolet radiation. Journal of Geophysical Research: Atmospheres, 126, e2021JD035079. https://doi.org/10.1029/2021JD035079
17. Neale, R. E., Barnes, P. W., Robson, T. M., et al. (2021). Environmental effects of stratospheric ozone depletion, UV radiation, and interactions with climate change: UNEP Environmental Effects Assessment Panel, Update 2020. Photochemical & Photobiological Sciences, 20, 1-67. https://doi.org/10.1007/s43630-020-00001-x
18. Osipov, S., Stenchikov, G., Tsigaridis, K., et al. (2021). The Toba supervolcano eruption caused severe tropical stratospheric ozone depletion. Communications Earth & Environment, 2, 71. https://doi.org/10.1038/s43247-021-00141-7

19. Tritscher, I., Pitts, M. C., Poole, L. R., Alexander, S. P., Cairo, F., Chipperfield, M. P., et al. (2021). Polar stratospheric clouds: Satellite observations, processes, and role in ozone depletion. Reviews of Geophysics, 59, e2020RG000702. https://doi.org/10.1029/2020RG000702
20. Park, S., Western, L. M., Saito, T., et al. (2021). A decline in emissions of CFC-11 and related chemicals from eastern China. Nature, 590, 433-437. https://doi.org/10.1038/s41586-021-03277-w
21. Feng, W., Dhomse, S. S., Arosio, C., Weber, M., Burrows, J. P., Santee, M. L., & Chipperfield, M. P. (2021). Arctic ozone depletion in 2019/20: Roles of chemistry, dynamics and the Montreal Protocol. Geophysical Research Letters, 48, e2020GL091911. https://doi.org/10.1029/2020GL091911
22. Tollefson, J. (2021). Illegal CFC emissions have stopped since scientists raised alarm. Nature, 590, 373. https://doi.org/10.1038/d41586-021-00360-0
23. Malinović-Milićević, S., Vyklyuk, Y., Stanojević, G., et al. (2021). Prediction of tropospheric ozone concentration using artificial neural networks at traffic and background urban locations in Novi Sad, Serbia. Environmental Monitoring and Assessment, 193, 84. https://doi.org/10.1007/s10661-020-08821-1
24. Gilik, A., Ogrenci, A. S., & Ozmen, A. (2021). Air quality prediction using CNN+LSTM-based hybrid deep learning architecture. Environmental Science and Pollution Research, 29, 11920–11938.
25. Narasimhan, D., & Vanitha, M. (2021). Ambient air quality assessment using ensemble techniques. Soft Computing, 25, 9943–9956. https://doi.org/10.1007/s00500-020-05470-x
26. Deng, T., Manders, A., Jin, J., & Lin, H. X. (2022). Clustering-based spatial transfer learning for short-term ozone forecasting. Journal of Hazardous Materials Advances, 8, 100168. https://doi.org/10.1016/j.hazadv.2022.100168
27. Chen, Y., Chen, X., Xu, A., et al. (2022). A hybrid CNN-Transformer model for ozone concentration prediction. Air Quality, Atmosphere & Health, 15, 1533–1546. https://doi.org/10.1007/s11869-022-01197-w
28. Tu, Z., & Wu, Z. (2022). Predicting Beijing air quality using Bayesian optimized CNN-RNN hybrid model. In 2022 Asia Conference on Algorithms, Computing and Machine Learning (CACML) (pp. 581–587). https://doi.org/10.1109/CACML55074.2022.00104

29. Zohdirad, H., Montazeri Namin, M., Ashrafi, K., et al. (2022). Temporal variations, regional contribution, and cluster analyses of ozone and NOx in a middle eastern megacity during summertime over 2017–2019. Environmental Science and Pollution Research, 29, 16233–16249. https://doi.org/10.1007/s11356-021-14923-1
30. He, H., Huang, Z., Xie, D., Liu, W., Huang, Z., Wang, X., Zhang, Y., Zhang, Z., Yang, L., Zhan, W., Peng, J., Huang, M., & Xu, M. (2023). Spatio-seasonal characterization and emissions estimation of ozone-depleting substances in the Pearl River Delta, China. Atmospheric Environment, 310, 119982. https://doi.org/10.1016/j.atmosenv.2023.119982
31. Li, Y., Jiang, T., Gu, H., Lu, W., Wu, Q., & Yu, Y. (2023). Air quality index prediction based on CNN-LSTM-attention hybrid modeling. In 2023 International Conference on the Cognitive Computing and Complex Data (ICCD) (pp. 175–180). https://doi.org/10.1109/ICCD59681.2023.10420640
32. Pradhan, S. S., Panigrahi, S., Purohit, S. K., & Dash, J. K. (2023). Study and development of hybrid and ensemble forecasting models for air quality index forecasting. Expert Systems, 40(10), e13449. https://doi.org/10.1111/exsy.13449
33. Lakshmipathy, M., Prasad, M. J. S., & Kodandaramaiah, G. N. (2024). Advanced ambient air quality prediction through weighted feature selection and improved reptile search ensemble learning. Knowledge and Information Systems, 66, 267–305. https://doi.org/10.1007/s10115-023-01947-x
34. Prakash, A., & Singh, S. K. (2024). CO2 emission prediction from coal used in power plants: A machine learning-based approach. Iranian Journal of Computer Science. https://doi.org/10.1007/s42044-024-00185-w
35. Gupta, S., Patel, N., Kumar, A., Jain, N. K., Dass, P., Hegde, R., & Rajaram, A. (2023). Adaptive fuzzy convolutional neural network for medical image classification. *Journal of Intelligent & Fuzzy Systems*, (Preprint), 1-17. **DOI:** 10.3233/JIFS-233819.
36. Ganiya, R. K., Veeraiah, D., Thatha, V. N., Rao, K. S., Rao, J. N., Manjith, R., & Rajaram, A. (2024). Revolutionizing vascular health through the temporal convolutional transformer for drug screening and model evolution. *Biomedical Signal Processing and Control*, *95*, 106390. https://doi.org/10.1016/j.bspc.2024.106390.

37. Chiranjeevi, P., & Rajaram, A. (2022). Twitter sentiment analysis for environmental weather conditions in recommendation of tourism. *Journal of Environmental Protection and Ecology*, *23*(5), 2113-2123.
38. Baskar, A., & Rajaram, A. (2022). Environment monitoring for air pollution control using multipath-based optimum routing in mobile ad hoc networks. *Journal of Environmental Protection and Ecology*, *23*(5), 2140-2149.
39. Saravanan, A., Farook, S., Kathir, I., Pushpa, S., Padmashini, R. K., Logeswaran, T., & Rajaram, A. (2024). Adaptive Solar Power Generation Forecasting using Enhanced Neural Network with Weather Modulation. *International Journal of Renewable Energy Research (IJRER)*, *14*(2), 275-292. https://doi.org/10.20508/ijrer.v14i2.14551.g8904.
40. Pushpavalli, M., Dhanya, D., Kulkarni, M., Rajitha Jasmine, R., Umarani, B., RamprasadReddy, M., ... & Rajaram, A. (2024). Enhancing Electrical Power Demand Prediction Using LSTM-Based Deep Learning Models for Local Energy Communities. *Electric Power Components and Systems*, 1-18. https://doi.org/10.1080/15325008.2024.2316246
41. Rajaram, A., Padmavathi, K., Ch, S. K., Karthik, A., & Sivasankari, K. (2024). Enhancing Energy Forecasting in Combined Cycle Power Plants using a Hybrid ConvLSTM and FC Neural Network Model. *International Journal of Renewable Energy Research (IJRER)*, *14*(1), 111-126. https://doi.org/10.20508/ijrer.v14i1.14591.g8880.
42. Chandrika, V. S., Kumar, N. M. G., Kamesh, V. V., Shobanadevi, A., Maheswari, V., Sekar, K., ... & Rajaram, A. (2024). Advanced LSTM-Based Time Series Forecasting for Enhanced Energy Consumption Management in Electric Power Systems. *International Journal of Renewable Energy Research (IJRER)*, *14*(1), 127-139. https://doi.org/10.20508/ijrer.v14i1.14561.g8868.
43. Pradeep, J., Raja Ratna, S., Dhal, P. K., Daya Sagar, K. V., Ranjit, P. S., Rastogi, R., ... & Rajaram, A. (2024). DeepFore: A Deep Reinforcement Learning Approach for Power Forecasting in Renewable Energy Systems. *Electric Power Components and Systems*, 1-17. https://doi.org/10.1080/15325008.2024.2332391.
44. Kamani, H., Baniasadi, M., Abdipour, H., Mohammadi, L., Rayegannakhost, S., Moein, H., & Azari, A. (2023). Health risk assessment of BTEX compounds (benzene, toluene,

ethylbenzene and xylene) in different indoor air using Monte Carlo simulation in zahedan city, Iran. *Heliyon*, *9*(9). https://doi.org/10.1016/j.heliyon.2023.e20294.

45. Delavari, M., Beyranvand, F., Jahangiri, M., & Abdipour, H. (2024). Increasing the permeability of carbon dioxide and nitrogen gases through a polymer membrane consisting of a modified polyether block amide and experimental design. *Journal of Polymers and the Environment*, *32*(10), 4822-4841. https://doi.org/10.1007/s10924-024-03247-z.
46. Kamani, H., Baniasadi, M., Abdipour, H., Mohammadi, L., Rayegannakhost, S., Moein, H., & Azari, A. (2023). Health risk assessment of BTEX compounds (benzene, toluene, ethylbenzene and xylene) in different indoor air using Monte Carlo simulation in zahedan city, Iran. *Heliyon*, *9*(9).
47. Delavari, M., Beyranvand, F., Jahangiri, M., & Abdipour, H. (2024). Increasing the permeability of carbon dioxide and nitrogen gases through a polymer membrane consisting of a modified polyether block amide and experimental design. *Journal of Polymers and the Environment*, *32*(10), 4822-4841.
48. Xiong, C., Tao, H., Liu, S., Liu, G., Wen, Z., Shang, Y., ... & Song, K. (2024). Using satellite imagery to estimate CO2 partial pressure and exchange with the atmosphere in the Songhua River. *Journal of Hydrology*, *634*, 131074.
49. Chen, L., Zhu, G., Lin, X., Li, R., Lu, S., Jiao, Y., ... & Wang, Q. (2024). The complexity of moisture sources affects the altitude effect of stable isotopes of precipitation in inland mountainous regions. *Water Resources Research*, *60*(6), e2023WR036084.
50. Feng, X., Wang, Z., Wu, X., Huang, S., Li, J., Lai, C., ... & Lin, G. (2025). Tracking 3D drought events across global river basins: Climatology, spatial footprint, and temporal changes. *Geophysical Research Letters*, *52*(3), e2024GL111442.
51. Gu, K., Liu, Y., Liu, H., Liu, B., Qiao, J., Lin, W., & Zhang, W. (2025). Air Pollution Monitoring By Integrating Local and Global Information in Self-Adaptive Multiscale Transform Domain. *IEEE Transactions on Multimedia*.
52. Li, B., Liu, Y., Zhao, X., Ning, P., Liu, X., & Zhu, T. (2021). O3 oxidation excited by yellow phosphorus emulsion coupling with red mud absorption for denitration. *Journal of Hazardous Materials*, *403*, 123971.

53. Tao, L., Wu, H., Wang, J., Li, B., Wang, X. Q., & Ning, P. (2019). Removal of SO2 from flue gas using Bayer red mud: Influence factors and mechanism. *Journal of Central South University*, *26*(2), 467-478.
54. Zhuo, T., He, L., Chai, B., Zhou, S., Wan, Q., Lei, X., ... & Chen, B. (2023). Micro-pressure promotes endogenous phosphorus release in a deep reservoir by favouring microbial phosphate mineralisation and solubilisation coupled with sulphate reduction. *Water Research*, *245*, 120647.
55. Huang, H., Liu, S., Kang, Z., Zhu, Y., Zhang, C., Xiang, E., ... & Liu, W. (2024). Effects of atmosphere and stepwise pyrolysis on the pyrolysis behavior, product characteristics, and N/S migration mechanism of vancomycin fermentation residue. *Chemical Engineering Journal*, *498*, 155012.